DOI: 10.17344/acsi.2023.8397 *Acta Chim. Slov.* **2024,** *71,* 20–25

Scientific paper

Synthesis, Crystal Structures and Antibacterial Activity of Nickel(II) and Copper(II) Complexes Derived from (*E*)-2-((2,3-dihydrobenzo[b][1,4]dioxin-6-yl)methylene)-*N*-phenylhydrazinecarbothioamide

Jing Wang[1], Haiyang Fei[1], Min Zhou[1], Chengcai Zhang[1], Juan Sun*[,2], Yang Zhou*[,3] and Meng Yang*[,1]

[1] *School of Pharmaceutical Engineering, Jiangsu Food & Pharmaceutical Science College, Huai'an 223005, China*

[2] *School of Biological & Chemical Engineering, Zhejiang University of Science & Technology, Hangzhou 310023, PR China*

[3] *Cixi Institute of Biomedical Engineering, Ningbo Institute of Materials Technology and Engineering, Chinese Academy of Sciences, Ningbo 315300, China*

** Corresponding author: E-mail: J. Sun (sunjuan18@zust.edu.cn); Y. Zhou (zhouyang876@nimte.ac.cn); M.Yang (yangmenghuaian@163.com)*

Received: 08-17-2023

Abstract

The biosynthesis of fatty acids is essential for the survival of bacteria, and *β*-ketoacyl-acyl carrier protein synthase III (FabH) is a promising target for antibacterial drug development. Nickel(II) complex [NiL_2] (**1**) and copper(II) complex [CuL_2] (**2**), where **L** is (*E*)-2-((2,3-dihydrobenzo[b][1,4]dioxin-6-yl)methylene)-*N*-phenylhydrazinecarbothioamide, were synthesized and characterized by elemental analysis, IR and ^{1}H NMR spectroscopy and HRMS. Structures of the complexes were further studied by single crystal X-ray determination, which reveals that the nickel and copper atoms in the complexes are in tetrahedral geometry. These compounds were evaluated for their antibacterial and *E. coli* FabH inhibitory activities.

Keywords: 1,4-Benzodioxane, nickel complex, copper complex, antibacterial activity, FabH inhibitory

1. Introduction

Coordination complexes have been extensively studied as potential inhibitors of FabH, a key enzyme involved in fatty acid biosynthesis.[1] FabH inhibitors have attracted significant attention as potential therapeutic agents for the treatment of bacterial infections.[2] Coordination complexes have been shown to inhibit FabH activity through a variety of mechanisms, including binding to the active site of the enzyme and disrupting its catalytic activity.[3] Some of the most promising complexes are those containing ruthenium, rhodium, cobalt, and platinum. For example, the Copper complexes have been shown to bind to the active site of FabH and inhibit its enzymatic activity.[4] Similarly, the cobalt and chromium complexes have also been shown to inhibit FabH activity.[5]

(*E*)-2-((2,3-dihydrobenzo[b][1,4]dioxin-6-yl)methylene)-*N*-phenylhydrazinecarbothioamide (**L**) is a potential antibacterial agent that belongs to the class of hydrazinecarbothioamide derivatives. It contains a dioxin ring system, a phenyl group, and a hydrazinecarbothioamide functional group, which are known to possess antibacterial activity.[6] The inhibitory activity of **L** against bacterial growth is believed to be due to its ability to target the FabH enzyme, which is essential for the biosynthesis of fatty acids in bacteria.[7] The compound binds to the active site of FabH and inhibits its activity, thereby preventing the production of fatty acids and disrupting bacterial growth. Overall, **L** has the potential to serve as a promising antibacterial skeleton for the development of new therapeutics targeting FabH.

The synthesis of new metal complexes with antibacterial properties is a prominent subject in the fields of coordination chemistry and bioinorganic chemistry.[8] Additionally, Ni and Cu metals are frequently employed in

coordination chemistry due to their well-documented biological activities, especially their antimicrobial properties.[9] Moreover, previous studies have demonstrated the effective interaction of metals with the active site of FabH, leading to interference with its enzymatic activity. Consequently, this study focuses on elucidating the crystal structures of nickel(II) and copper(II) complexes with the ligand **L**, as well as examining their antibacterial and FabH inhibitory activities. These findings provide valuable insight into the potential clinical application of the hydrazinecarbothioamide complex as an antibacterial agent.

2. Experimental

2. 1. Materials and Methods

1,4-benzodioxane-6-formaldehyde, nickel acetate, copper acetate, hydrazine hydrate and phenyl isothiocyanate were obtained from Aladdin. All other chemicals were commercial obtained from Anhui Senrise Technologies Co., Ltd. HNMR spectra were measured on a Bruker AV-400 spectrometer at 25 °C and referenced to Me_4Si. LC/MS spectra were recorded on a Waters G2-XSQTot Mass spectrometer. Chemical shifts were reported in ppm (δ) using the residual solvent line as internal standard. Analytical thin-layer chromatography (TLC) was performed on the glassbacked silica gel sheets (silica gel 60 Å GF254). Elemental analyses for C, H and N were performed on a Perkin-Elmer 240C elemental analyzer. FT-IR spectra were obtained on BrukerVertex 70 with samples prepared as KBr pellets. Single crystal X-ray diffraction was carried out on a Bruker SMART 1000 CCD diffractometer.

2. 2 Synthesis of (*E*)-2-((2,3-dihydrobenzo[b][1,4]dioxin-6-yl)methylene)-*N*-phenylhydrazinecarbothioamide (L)

1,4-benzodioxane-6-formaldehyde (0.16 g, 1.0 mmol) and hydrazine hydrate (0.13 g, 4.0 mmol) were mixed in 30 mL ethanol. The mixture was reflux for 4 h and the solvent was evaporated to give solid product **b**, which was re-crystallized from ethanol, yield 95%. Then the intermediate hydrazine compound **b** (0.14 g, 0.8 mmol) and phenyl isothiocyanate (0.14 g, 1 mmol) was dissolved in chloroform (30 mL) and refluxed for 4 h. The solvent was evaporated under reduced pressure, and the ligand **L** was obtained by recrystallized from ethanol. ^{1}H NMR (400 MHz, DMSO-*d6*) *δ* 11.69 (s, 1H), 10.07 (s, 1H), 8.03 (s, 1H), 7.60–7.52 (m, 3H), 7.36 (m, 2H), 7.28 (m, 1H), 7.20 (m, 1H), 6.89 (d, *J* = 8.3 Hz, 1H), 4.27 (m, 4H). ^{13}C NMR (101 MHz, DMSO-*d6*) *δ* 176.20, 145.79, 144.16, 143.11, 139.61, 128.46, 127.88, 126.44, 125.72, 122.31, 117.62, 115.96, 64.79, 64.44. Anal. calc. for $C_{16}H_{15}N_3O_2S$: C, 61.32; H, 4.82; N, 13.41; found: C, 61.17; H, 4.95; N, 13.56%. HR-MS m/z: 314.0954 $(M+H)^+$, calculated molecular weight of $C_{16}H_{16}N_3O_2S^+$: 314.0885 for $(M+H)^+$.

2. 3. Synthesis of $[NiL_2]$ (1)

L (0.10 mmol) and nickel acetate (0.10 mmol) mixed in methanol (10 mL) were stirred at room temperature for 30 min to give a clear earthy yellow solution. Needle-shaped dark purple crystals suitable for X-ray diffraction were grown from the solution upon slowly evaporation within 2 days. The crystals were isolated by filtration. ^{1}H NMR (400 MHz, DMSO-*d6*) *δ* 9.71 (s, 1H), 7.96 (d, *J* = 2.0 Hz, 1H), 7.74 – 7.47 (m, 4H), 7.30 (m, 2H), 7.02 (m, 1H), 6.87 (d, *J* = 8.5 Hz, 1H), 4.50–4.16 (m, 4H). Anal. calc. for $C_{32}H_{28}N_6NiO_4S_2$: C, 56.24; H, 4.13; N, 12.30; found: C, 56.12; H, 4.27; N, 12.21%. HR-MS m/z: 683.1014$(M+H)^+$, calculated molecular weight of $C_{32}H_{29}N_6NiO_4S_2^+$: 683.0967 for $(M+H)^+$.

2. 3. Synthesis of $[CuL_2]$ (2)

L (0.10 mmol) and copper acetate (0.10 mmol) mixed in methanol (10 mL) were stirred at room temperature for 30 min to give a clear green solution. Half of the solvent was slowly evaporated at room temperature for 6 days to give single crystals. Anal. calc. for $C_{32}H_{28}N_6CuO_4S_2$: C, 55.84; H, 4.10; N, 12.21; found: C, 565.76; H, 4.25; N, 12.16%. IR data (cm^{-1}): 3474, 3146, 1541, 1509, 1421, 1294, 1063, 963, 811, 679, 626, 553. HR-MS m/z: 688.0915$(M+H)^+$, calculated molecular weight of $C_{32}H_{29}N_6CuO_4S_2^+$: 688.0909 for $(M+H)^+$.

2. 4. X-ray Crstallography

X-ray diffraction was carried out at a Bruker APEX II CCD area diffractometer equipped with MoK*α* radiation (*λ* = 0.71073 Å). The collected data were reduced with SAINT,[10] and multi-scan absorption correction was performed using SADABS. [11] The structures of the complexes were solved by direct method, and refined against *F*2 by full-matrix least-squares method using SHELXTL.[12] For Cu complex, there is a thermal vibration in the crystal as a whole, so during refinement, the center Cu is fixed and all organic frameworks complexed with Cu are subjected to disordered treatment. The SIMU command allows for the simultaneous optimization of multiple atoms, ensuring the coordination geometry around Cu is accurately represented. The SADI command is employed to constrain the bond length variations between specific atoms, ensuring consistent bond lengths within the complex. Lastly, the ISOR command helps model the thermal vibrations of atoms by assigning isotropic displacement parameters to capture their positional uncertainties. The ultimate goal of related instructions is to make refinement more perfect and to make the structure converge. Crystallographic data and refinement parameters are given in Table 1, and important interatomic distances and angles are given in Table 2.

2. 5. Antibacterial Assay

The in vitro minimal inhibitory concentrations (MICs) of the synthesized derivatives were obtained

against two clinical Gram-positive bacterial strains: *Bacillus subtilis* (*B. subtilis*), *Staphylococcus aureus* (*S. aureus*) and two clinical Gram-negative bacterial strains: *Pseudomonas aeruginosa* (*P. aeruginosa*), *Escherichia coli* (*E. coli*) by the agar dilution method recommended by Clinical and Laboratory Standards Institute (CLSI) (CLSI 2012). The MIC was the lowest concentration in solid media at which no bacterial growth was observed.

2. 6. Enzyme Assay

The experiments were performed according to the previous reports.[13] In a final 20 μL reaction, 20 mM Na_2HPO_4 containing 0.5 mM DTT, 0.25 mM $MgCl_2$, and 2.5 μM holo-ACP were mixed with 1 nM FabH, and H_2O was added to 15 μL. After 1 min incubation, a 2 μL mixture of 25 μM acetyl-CoA, 0.5 mM reduced nicotinamide adenine dinucleotide (NADH), and 0.5 mM reduced nicotinamide adenine dinucleotide phosphate (NADPH) was added for FabH reaction for 25 min. The reaction was stopped by adding 20 μL of ice-cold 50% trichloroacetic acid (TCA), incubating for 5 min on ice, and centrifuging to pellet the protein. The pellet was washed with 10% ice-cold TCA and resuspended with 5 µL of 0.5 M NaOH. The incorporation of the ^3H signal in the final product was read by liquid scintillation. When determining the inhibition constant (IC_{50}), inhibitors were added from a concentrated DMSO stock such that the final concentration of DMSO did not exceed 2%.

3. Results and Discussion

3. 1. Chemistry

Synthetic route of the ligand (**L**) was shown in Scheme 1. 1,4-benzodioxane-6-formaldehyde reacts with hydrazine hydrate in ethanol solution to form 1,4-benzodioxane-hydrazine, and then the intermediate hydrazine compound is stirred with phenyl isothiocyanate in methanol solution to form the final ligand **L**. Finally, the ligand **L** and nickel acetate or copper acetate reacted in the ratio of 2:1 separately to get the complex **1** and **2** in ethanol. Single crystals of the complexes were formed by slow evaporation of the solvent at room temperature.

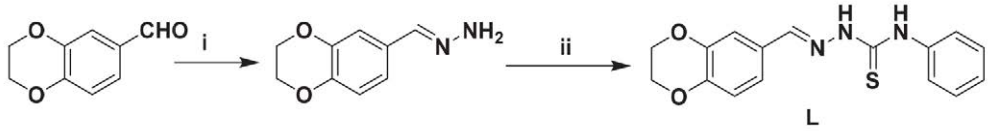

Reagents and conditions: (i) $NH_2NH_2 \cdot H_2O$, ethanol, reflux; (ii) Phenyl isothiocyanate, chloroform, reflux

Scheme 1. Synthetic route of Ligand **L**.

3. 2. Structure Description of Complex 1

Selected bond lengths and angles for complex **1** are listed in Table 2. Molecular structure of the complex is shown in Figure 1. The Ni atom is coordinated in square planar geometry, with two S and two imino N atoms from two ligands. The coordination geometry around the Ni1 atom exhibits a planar–square arrangement. Both ligands attached to Ni demonstrate a perfectly symmetric structure. Furthermore, it is evident that the N3–Ni1–N3^1 angle is 180°, similarly, the S1^1–Ni1–S1 angle also measures 180°. Additionally, the Ni1 -S1 bond length is determined to be 2.181(2) Å, while the Ni1–N3 bond length measures 1.915(6) Å, consistent with the expected values.

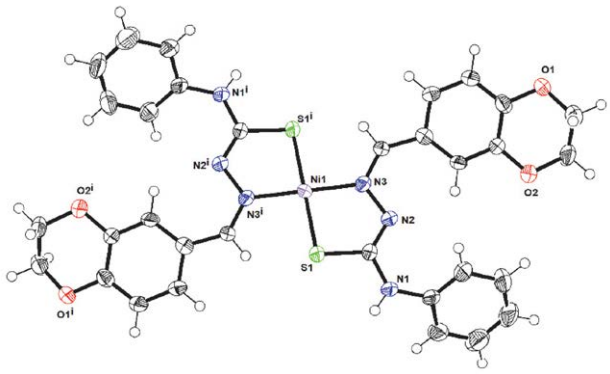

Figure 1. A perspective view of the molecular structure of complex **1** with the atom labeling scheme.

3. 3. Structure Description of Complex 2

Selected bond lengths and angles for complex **1** are listed in Table 2. Molecular structure of the complex is shown in Figure 2. The spatial arrangement of compound **2** distinguishes it from compound **1**, as evidenced by the crystallographic characterization provided in Figure 2. Notably, the Cu1 atom in compound **2** deviates from planar-square coordination, exhibiting a discernible angular distortion. The confirmation of this deviation stems from the measured S1–Cu1–S2 angle of 174.6 degrees and the N3–Cu1–N4 angle of 167.5 degrees. Additionally, despite the consistent selection of ligands forming metal bonds with Cu^{2+} in compound **2**, the coordinated ligands do not maintain symmetrical structures around the central Cu atom. This asymmetry is substantiated by the determined bond lengths between the ligands and the metal ion: Cu1–S1 measures 2.185(13) Å, Cu1–S2 measures 2.258(13) Å, Cu1–N3 measures 1.85(2) Å, and Cu1–N4 measures 2.215(19) Å.

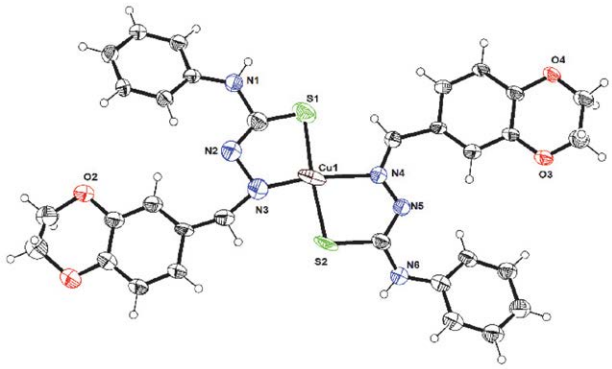

Figure 2. A perspective view of the molecular structure of complex **2** with the atom labeling scheme.

The origin of this asymmetric coordination of ligands to the copper ion lies in the influence of their orientations and conformations within the molecular framework. While the ligands themselves possess inherent symmetry, their coordination to the metal center can occur in variable orientations, thus culminating in an overall loss of symmetry within the complex. The disruption of symmetry observed in the compound can be attributed to multiple factors, including the orientation and localized distortion of the ligands. The presence of neighboring molecules or ligands may induce perturbations, leading to local distortions upon coordination with the metal ion. These distortions contribute to spatial asymmetry within the system. Additionally, the conformational flexibility of the ligands plays a significant role in symmetry disruption. Despite sharing the same chemical formula, the ligands may exhibit diverse conformations, influenced by freely rotating bonds or other conformational degrees of freedom. This inherent flexibility allows the ligands to adopt different coordination modes when binding to the metal center, further exacerbating the overall structural asymmetry. Consequently, the investigation and comprehension of this asymmetry necessitate in-depth exploration via comprehensive structural analysis and sophisticated computational methods.

Table 2. Selected bond lengths (Å) and angles (°) for complexes

1			
Ni1–S1^{I}	2.181(2)	Ni1–N3^{I}	1.915(6)
Ni1–S1	2.181(2)	Ni1–N3	1.915(6)
S1^{1}–Ni1–S1	180.0	N3–Ni1–S1^{1}	94.42(17)
N3–Ni1–S1	85.57(17)	N3^{1}–Ni1–S^{1}	94.42(17)
N3^{1}–Ni1–S1^{1}	85.57(17)	N3–Ni1–^{N}31	180.0
2			
Cu1–S1	**2.185(13)**	**Cu1–N3**	**1.85(2)**
Cu1–S2	2.258(13)	Cu1–N4	2.215(19)
S1–Cu1–S2	174.6(8)	S1–Cu1–N4	94.6(8)
N4–Cu1–S2	80.2(7)	N3–Cu1–S2	88.5(9)
N3–Cu1–S1	96.6(11)	N3–Cu1–N4	167.5(11)

3. 4. Biological Activity

The MIC (Minimum inhibitory concentration, μM) of complex **1** and complex **2** against these bacterial strains

Table 1. Crystallographic and refinement data for the complexes

Complexes	**1**	**2**
Empirical Formula	$C_{32}H_{28}N_6NiO_4S_2$	$C_{32}H_{28}CuN_6O_4S_2$
Formula Weight	683.43	688.26
Crystal System	Triclinic	Monoclinic
Space group	*P*–1	*Cc*
a (Å)	6.570(4)	19.396(3)
b (Å)	7.296(5)	17.857(3)
c (Å)	16.768(10)	8.6520(13)
α (°)	85.557(18)	90
β (°)	80.676(18)	95.578(4)
γ (°)	69.897(18)	90
V (Å^3)	744.6(8)	2982.5(8)
Z	1	4
D_c (g cm^{-3})	1.524	1.533
F(000)	354	1420
μ(Mo-Kα) (mm^{-1})	0.842	0.922
Reflections collected	6565	12152
Data/restraints/parameters	2556/0/205	5060/2208/709
Independent reflections (R_{int})	2556 (0.0703)	5060 (0.0657)
Goodness-of-fit on F^2	1.037	1.027
Final R_1, wR_2 indexes [$I >= 2\sigma$ (I)]	0.0780, 0.1930	0.0768, 0.1339
Final R_1, wR_2 indexes [all data]	0.1504, 0.2661	0.1959, 0.1765

are tested by MTT method and the activity data was presented in Table 3. Based on the data obtained, we found that the two compounds showed some inhibitory activity. In particular, the inhibitory effect on Gram-negative bacteria was significantly stronger than that of Gram-positive bacteria, and the inhibitory activity was comparable to the positive control kanamycin. Among them, complex **2** has the highest inhibitory activity against two Gram-negative bacteria (MIC = 3.13 μM for *P. aeruginosa*, MIC = 2.5 μM for *E. coli*).

Table 3. Antibacterial activity of synthetic complex **1** and **2**.

Compound	Minimum inhibitory concentration, μM			
	Gram-negative		Gram-positive	
	E. coli	*P. aeruginosa*	*B. subtilis*	*S. aureus*
1	6.25	6.25	12.5	12.5
2	2.5	3.13	6.25	12.5
kanamycin	2.5	2.5	2.5	1.25

E. coli FabH inhibition potency of complex **1** and complex **2** was examined and the results are summarized in Table 4. As shown in Table 4, all of the two compounds tested exhibited a certain inhibitory activity against *E. coli* FabH wherein the compound having the highest inhibitory activity remained complex **2** (IC_{50} = 3.67 μM). This result indicates that the 1 *E*)-2-((2,3-dihydrobenzo[b][1,4] dioxin-6-yl)methylene)-*N*-phenylhydrazinecarbothioamide complexes can inhibit the function of FabH and the antibacterial effect was produced partly by interaction of FabH protein and the compounds.

Table 4. *E. coli* FabH inhibitory activity of synthetic complex **1** and **2**.

Compound	*E. coli* FabH (IC_{50}±SD), μM
1	10.15±0.329
2	3.67±0.165

3. Conclusions

In this manuscript, we describe a novel hydrazinecarbothioamide metal complex and present our findings on its crystal structures, antibacterial activity, and FabH inhibitory activity. Our results demonstrate that Complex **2** exhibits effective inhibition of FabH activity against *E. coli*, indicating its potential as a novel FabH inhibitor.

Coordination complexes as FabH inhibitors have high surface area-to-volume ratios and heterogeneity, which can enhance their biological availability and efficacy. However, more studies are needed to evaluate their safety and bioavailability before they can be developed into therapeutic agents. Future studies could focus on optimizing the pharmacological properties and antimicrobial activity of these complexes, as well as exploring their potential as therapeutic agents for the treatment of bacterial infections.

Acknowledgement

This work was supported by Natural science research plan of Huai'an City (HAB202146); Jiangsu Higher Education Institutions Basic Science (Natural Science) General Program（22KJD150004）and Qing Lan Project; the S&T Innovation 2025 Major Special Program of Ningbo (2020Z091).

Conflict of Interest

The authors declare no conflict of interest.

Supplementary Data

CCDC 2266563 (**1**) and 2266562 (**2**) contain the supplementary crystallographic data for the compounds. These data can be obtained free of charge *via* http://www.ccdc.cam.ac.uk/conts/retrieving. html, or from the Cambridge Crystallographic Data Centre, 12 Union Road, Cambridge CB2 1EZ, UK; fax: (+44) 1223-336-033; or e-mail: deposit@ccdc.cam.ac.uk. The spectral data of the compounds can be found in the supporting information file.

5. References

1. (a) A. S. Orabi, K. M. Abou EI-Nour, M. F. Youssef, H. A. Salem, *Arab. J. Chem*. **2020**, *13*, 2628-2648. **DOI:**10.1016/j.arabjc.2018.06.016
(b) A. M. Abbas, S. R. Fisal, A. S. Radwan, M. M. Makhlouf, A. S. Orabi, *J. Mol. Liq*. **2022**, *351*, 118333. **DOI:**10.1016/j.molliq.2021.118333
2. (a) H. J. Zhang, Z. L. Li, H. L. Zhu, *Curr. Med. Chem*. **2012**, *19*, 1225-1237. **DOI:**10.2174/092986712799320484
(b) Y. Zhou, Y. Q. Liang, X. Y. Wang, H. Y. Chang, S. P. Hu, J. Sun, *Chem. Pharm. Bull*. **2022**, *70*, 544-549. **DOI:**10.1248/cpb.c22-00090
(c) H. Song, G. Z. Ao, H. Q. Li, *Expert. Opin. Ther. Pat*. **2013**, *24*, 19-27. **DOI:**10.1517/13543776.2014.847091
(d) A. Mittal, M. E. Johnson, *J. Mol. Graph. Model*. **2015**, *55*, 115-122. **DOI:**10.1016/j.jmgm.2014.11.004
3. (a) S. Altaf, A. Haider, S. Naz, A. UI-Hamid, J. Haider, M. Imran, A. Shahzadi, M. Naz, H. Ajaz, M. Ikram, *Nanoscale. Res. Lett*. **2020**, *15*, 144. **DOI:**10.1186/s11671-020-03375-0
(b) A. S. Reddy, J. C. Mao, S. Vanitha, V. N. Badavath, L. S. Krishna, M. Lavanya, M. V. J. Kumar, *J. Saudi. Chem. Soc*. **2019**, *23*, 947-957. **DOI:**10.1016/j.jscs.2019.04.003
4. S. I. Khan, S. Ahmad, A. A. Altaf, M. K. Rauf, A. Badshah, S.

S. Azam, M. N. Tahir, *New. J. Chem.* **2020**, *43*, 19318-19330. **DOI:**10.1039/C9NJ03005K
5. T. Rohand, H. B. E. Ayouchia, H. Achtak, A. Ghaleb, Y. Derin, A. Tutar, K. Tanemura, *J. Biomol. Struct. Dyn.* **2021**, *40*, 11837-11850. **DOI:**10.1080/07391102.2021.1965031
6. (a) E. D. Dincel, G. N. Ulusoy, D. Satana, O. Kucukbasmaci, *J. Heterocyclic. Chem.* **2020**, *58*, 195-205. **DOI:**10.1002/jhet.4159
(b) E. Pahontu, L. Socea, S. F. Barbuceanu, D. Ilies, M. Badea, O. T. Olaru, A. Gulea, B. Socea, O. Bratu, *Rev. Chim*. **2018**, *69*, 2959-2963. **DOI:**10.37358/RC.18.11.6662
(c) E. D. Dincel, C. Akdag, T. Kayra, E. D. Cosar, M. O. Aksoy, G. Akalin-Ciftci, N. Ulusoy-Guzeldemirci, *J. Mol. Struc*t. **2022**, *1268*, 133710. **DOI:**10.1016/j.molstruc.2022.133710
7. V. V. Salian, B. Narayana, B. K. Sarojini, M. S. Kumar, K. S. Chandra, A. G. Lobo, *J. Mol. Struc*t. **2019**, *1192*, 91-104. **DOI:**10.1016/j.molstruc.2019.04.105
8. W. G. Zhang, *Acta Chim. Slov*. **2023**, *70*, 421–429. **DOI:**10.17344/acsi.2023.8144
9. (a) L. Zhang, X.Y. Qiu, S. J Liu, *Acta Chim. Slov.* **2023**, *70*, 12–20. **DOI:**10.17344/acsi.2022.7737
(b) Y. M. Hao, *Acta Chim. Slov*. **2023**, *70*, 327–332. **DOI:**10.17344/acsi.2023.8104
(c) J. Jiang, P. Liang, Y. X. Han, H. Zhang, Z. L. You, *Acta Chim. Slov*. **2023**, *70*, 353–360. **DOI:**10.17344/acsi.2023.8253
10. Bruker, SMART and SAINT, Bruker AXS Inc., Madison, **2002**.
11. G. M. Sheldrick. SADABS, University of Göttingen, Germany, **1996**.
12. G. M. Sheldrick, *Acta Crystallogr*. **2015**, *C71*, 3–8.
13. J. Sun, C. P. Zhang, C. H. Chen, X. M. Guo, C. S. Liu, Y. Zhou, F. L. Hu, *Chem. Biodivers*. **2023**, *20*, e202201060. **DOI:**10.1002/cbdv.202201060

Povzetek

Biosinteza maščobnih kislin je bistvenega pomena za preživetje bakterij, β-ketoacil-acyl transportni protein sintaza III (FabH) pa je obetavna tarča za razvoj antibakterijskih učinkovin. Nikljev(II) kompleks [NiL_2] (**1**) in bakrov(II) kompleks [CuL_2] (**2**), kjer je *L* (*E*)-2-((2,3-dihidrobenzo[b][1,4]dioksin-6-il)metilen)-*N*-fenilhidrazinkarbotioamid, sta bila sintetizirana in okarakterizirana z elementarno analizo, IR in ^{1}H NMR spektroskopijo ter HRMS. Strukture kompleksov so bile določene z monokristalno rentgensko analizo, ki razkriva, da so nikljevi in bakrovi atomi v kompleksih v tetraedrični geometriji. Določili smo antibakterijsko in FabH inhibitorno delovanje teh dveh spojin na *E. coli*.